

Notch signaling enhances bone regeneration in the zebrafish mandible

Jessica M. Kraus¹, Dion Giovannone², Renata Rydzik¹, Jeremy L. Balsbaugh³, Isaac L. Moss¹, Jennifer L. Schwedler⁴, Julien Y. Bertrand⁴, David Traver⁴, Kurt D. Hankenson⁵, J. Gage Crump² and Daniel W. Youngstrom^{1,*}

ABSTRACT

Loss or damage to the mandible caused by trauma, treatment of oral malignancies, and other diseases is treated using bone-grafting techniques that suffer from numerous shortcomings and contraindications. Zebrafish naturally heal large injuries to mandibular bone, offering an opportunity to understand how to boost intrinsic healing potential. Using a novel *her6:mCherry* Notch reporter, we show that canonical Notch signaling is induced during the initial stages of cartilage callus formation in both mesenchymal cells and chondrocytes following surgical mandibulectomy. We also show that modulation of Notch signaling during the initial post-operative period results in lasting changes to regenerate bone quantity one month later. Pharmacological inhibition of Notch signaling reduces the size of the cartilage callus and delays its conversion into bone, resulting in non-union. Conversely, conditional transgenic activation of Notch signaling accelerates conversion of the cartilage callus into bone, improving bone healing. Given the conserved functions of this pathway in bone repair across vertebrates, we propose that targeted activation of Notch signaling during the early phases of bone healing in mammals may both augment the size of the initial callus and boost its ossification into reparative bone.

KEY WORDS: Bone, Osteoblasts, Notch signaling, Fracture healing, Regeneration, Zebrafish

INTRODUCTION

Although bone has some degree of intrinsic healing ability, humans lack the capacity for large-scale skeletal regeneration following major trauma. Surgical resection and/or reconstruction of the mandible is indicated for numerous clinical problems, including primary oral cancers with bony invasion (Shah and Gil, 2009); 25% of patients with oral squamous cell carcinoma are treated with segmental mandibulectomy (Rogers et al., 2004). High-energy trauma (Vaca et al., 2018), osteomyelitis (Marschall et al., 2019),


antiresorptive-related osteonecrosis (Khan et al., 2015) and elective orthognathic correction (Alyahya and Swennen, 2019) constitute other indications. The current standard of care for reconstruction of segmental mandible defects is the vascularized free fibular flap (Kim et al., 2013), which provides bony continuity at the expense of increased mortality, increased pain and decreased quality of life (Rogers et al., 2004). There is a significant unmet clinical need for regenerative therapies to augment bone healing, particularly for craniofacial applications for which form is linked not only to function, but also to social competence and mental health (Snyder et al., 2005). Moreover, ageing, radiation/chemotherapy (Hoff et al., 2008) and polytrauma (King et al., 2004) are common co-morbid risk factors for non-union in this patient population. To improve our understanding of how to boost endogenous bone healing, we investigated mandibular healing in an organism that naturally regenerates such defects without exogenous intervention.

Zebrafish (*Danio rerio*) are an ideal companion model organism to laboratory mice (Busse et al., 2020), in part because of an abundance of molecular and genetic tools, high throughput, and low cost. Similar to the mouse, approximately 70% of all human genes and 80% of disease-causing genes have a zebrafish ortholog (Howe et al., 2013), and zebrafish have cellular skeletons with all human bone cell types (Bergen et al., 2019). Despite this high degree of genetic conservation, and in contrast to mammals, zebrafish are capable of exceptional bone healing, including appendicular regeneration following amputation (Pfefferli and Jazwińska, 2015). The adult caudal fin undergoes epimorphic regeneration in 2-3 weeks following near-complete amputation, an observation reported in the 18th century (Broussonet, 1789) but now understood with increasingly sophisticated cellular and molecular resolution. Fin ray bones regenerate through both dedifferentiation of existing osteoblasts (Knopf et al., 2011) and transdifferentiation of intra-ray fibroblasts (Singh et al., 2012), highlighting the complex nature of skeletal regeneration in zebrafish.

We have reported that the zebrafish mandible is capable of large-scale bone regeneration in adults (Paul et al., 2016). The mandible is developmentally derived from cranial neural crest cells of the first pharyngeal arch (Schilling et al., 1996). Regeneration of the mandibular bone occurs through the formation of cells with a hybrid phenotype between cartilage and bone, with the morphological cartilage callus directly transforming into bone. Similar hybrid cartilage-bone cells have been observed in regeneration of the murine rib bone: one of the few bones in mammals capable of larger-scale regeneration (Kuwahara et al., 2019). Hedgehog signaling in *Sox9*-expressing periosteal cells promotes mineralization of this hybrid callus (Paul et al., 2016). However, our understanding of the pathways regulating the formation and maturation of the regenerative fracture callus is still incomplete.

¹Department of Orthopaedic Surgery, University of Connecticut Health Center, Farmington, CT 06030, USA. ²Department of Stem Cell Biology and Regenerative Medicine, Keck School of Medicine of the University of Southern California, Los Angeles, CA 90033, USA. ³Proteomics & Metabolomics Facility, Center for Open Research Resources & Equipment, University of Connecticut, Storrs, CT 06269, USA. ⁴Section of Cell and Developmental Biology, University of California San Diego, La Jolla, CA 92093, USA. ⁵Department of Orthopaedic Surgery, University of Michigan Medical School, Ann Arbor, MI 48109, USA.

*Author for correspondence (dwyoungstrom@uchc.edu)

 J.M.K., 0000-0001-7890-0613; J.L.B., 0000-0002-1852-8749; J.Y.B., 0000-0001-6570-4082; D.T., 0000-0002-9652-7653; K.D.H., 0000-0001-6361-143X; J.G.C., 0000-0002-3209-0026; D.W.Y., 0000-0002-1193-8868

Alagille syndrome (Li et al., 1997), primarily caused by heterozygosity of loss-of-function mutations in jagged 1 (*JAG1*; the most abundant Notch ligand in bone) results in decreased bone mass (Olsen et al., 2005), pathologic extremity fractures (Bales et al., 2010) and characteristic midfacial hypoplasia (Oda et al., 1997). Conditional genetic mouse models targeting *Jag1* in neural crest cells (Hill et al., 2014; Humphreys et al., 2012) and in osteoblasts (Youngstrom et al., 2016) recapitulate many of these skeletal abnormalities. Ongoing pre-clinical investigations by our group (Youngstrom et al., 2017) and others (Kamalakar et al., 2021; Novak et al., 2020) suggest that Notch signaling agonists can improve bone healing outcomes in mice. This prompted us to study the function of this pathway during the formation of regenerative osteochondral mesenchyme in zebrafish.

Notch signaling has been previously implicated in zebrafish caudal fin regeneration, a condition in which *jag1a* and *her6* (orthologous to human *HES1*) are highly expressed (Schebesta et al., 2006). In this model, Notch1a signaling functions to maintain bone-derived blastema cells in a proliferative and undifferentiated state (Grotek et al., 2013), and regulates formation and remodeling of the supporting vascular plexus (Kametani et al., 2015). Whereas dedifferentiated osteoblasts are responsible for intramembranous bone regeneration at numerous skeletal sites in zebrafish (Geurtzen et al., 2014), chondroid regeneration of the mandible is mechanistically distinct. To investigate the function of Notch signaling within adult mandibular defect healing, we used pharmacological and genetic approaches to modify Notch signaling following experimental mandibulectomy. We find that Notch signaling is required for cartilage callus formation, and that augmented Notch signaling early in repair can improve mandibular bone regeneration, likely by accelerating the conversion of the hybrid cartilage callus to bone.

RESULTS AND DISCUSSION

Activation of Notch signaling during mandible regeneration

We produced a novel transgenic reporter fish harnessing the promoter of *her6*, a direct transcriptional target of canonical Notch receptor signaling. We verified overlap between the *her6:mCherry* reporter and the endogenous Notch1a intracellular domain (NICD) at 10 days post-resection (dpr) at the injury margin by immunohistochemistry (IHC) (Fig. 1A). To understand the temporal regulation of Notch signaling in the context of mandible regeneration, *her6:mCherry* animals subjected to unilateral mandibulectomy were harvested for histological analyses (Safranin O staining and mCherry IHC) at 0, 4, 7, 10 and 14 dpr (Fig. 1B). At 0 dpr, *her6:mCherry*⁺ cells were visible in the skin, weakly within Meckel's chondrocytes, and among the stromal cells on the medial aspect of the Meckel's cartilage. Between 4 and 7 dpr, a small number of *her6:mCherry*⁺ cells were visible lining the bone injury margins. At 10 dpr, the strongest *her6:mCherry* activity was observed in condensations of repair chondroblasts, as well as among the majority of the fibroblastic mesenchyme. *her6:mCherry* reporter activity began to wane at 14 dpr as the callus matured.

Because the greatest *her6:mCherry* activity was observed by IHC at 10 dpr, this time point was selected for subsequent bulk gene expression analysis by quantitative polymerase chain reaction (qPCR) (Fig. 1C). The 10 dpr callus is a highly dynamic and heterogeneous environment and, relative to paired intact contralateral mandibles, upregulation of numerous endochondral, matrix/remodeling and Notch-associated genes was observed. For example, *sox9a* was upregulated 3.16±1.68-fold ($P=0.028$), *coll1a2*

was upregulated 4.80±3.45-fold ($P=0.007$), *sp7* was upregulated 3.48±1.40-fold ($P=0.003$) and *tnc* was upregulated 6.50±3.25-fold ($P=0.002$). Upregulation of *bglap* did not reach statistical significance ($P=0.059$), but *spp1* did ($P=0.043$). Analogous to our understanding of mammalian bone (Youngstrom et al., 2017), *jag1b* was the most abundantly expressed ligand in both the resected and contralateral mandible samples. However, *jag2b* and *dlc* were upregulated in the context of injury, whereas *jag1b* was not. *notch1a* was the only receptor to be significantly upregulated within the mandible callus. Notch ligands/receptors listed in Table S1 but not reported in Fig. 1C were below the limit of detection by qPCR. These data associate Notch signaling with the early healing response following segmental mandibulectomy.

Notch signaling is necessary for mandible regeneration

To test the hypothesis that postoperative Notch signaling directly regulates mandible regeneration, complementary strategies were used to block and over-activate this pathway (Fig. 2A). In one experiment, three 16-h treatments of 20 μM dibenzazepine (DBZ) in dimethyl sulfoxide (DMSO) vehicle were used to pharmacologically inhibit activation of all Notch receptors every 48 h beginning 4 h post-resection. To conditionally overexpress the active NICD in all tissues using the Gal4/UAS system, *hsp:NICD* fish were treated with three 30-min heat shocks every 48 h beginning 2 h prior to surgery. DMSO-treated fish or *hsp:NICD(-)* fish subjected to the same heat-shock regimens were used as controls for each experiment, respectively.

X-ray microtomography (μCT) analysis of the callus at 32 dpr revealed striking differences in regenerate bone quantity, which were proportional to post-operative Notch signaling levels (Fig. 2B). DBZ treatment resulted in 58.6% less bone volume (BV) ($P=0.017$), 57.3% less bone surface area (BS) ($P=0.007$) and 59.5% less tissue mineral content (TMC) ($P=0.018$) relative to DMSO-treated siblings. This phenotype was even more severe in magnitude when DBZ treatment was consolidated into single 48-h treatments targeted within a range of times between 0 and 5 dpr (Fig. S1). Although the 48-h treatments were not powered to detect significant differences from each other, the 1-3 dpr treatment window had the lowest mean BV. In contrast to the reductions in regenerate bone observed following DBZ treatment, heat-shocked *hsp:NICD*⁺ animals acquired 89.6% more BV ($P=0.013$), 69.7% more BS ($P=0.020$), and 87.9% more TMC ($P=0.019$) relative to heat shocked *hsp:NICD(-)* siblings. Tissue mineral density (TMD) was not changed in either experiment, indicating that post-operative Notch signaling regulates quantity but not quality of regenerate bone tissue at 32 dpr.

Phenotypically wild-type animals generally achieve filling of the defect space with bone by 32 dpr. Perturbations of the Notch pathway in the early post-operative period interfered with this month-long process. DBZ treatment resulted in mandible non-union, whereas NICD overexpression increased bone formation. Fig. 2C,D depicts representative low- and high-healers in each group/experiment at 32 dpr. Incidentally, we also identified increased bone mass in T1 vertebral bodies of *hsp:NICD*⁺ animals (Fig. S2), suggesting global changes to skeletal metabolism.

Early Notch receptor inhibition results in stunted regeneration and non-union

To characterize further the DBZ-induced reduction in regenerative bone formation in *her6:mCherry* animals, Safranin O histology and mCherry IHC was performed on tissue sections from DMSO- and DBZ-treated animals (Fig. 3A,B). At 10 and 18 dpr, significantly

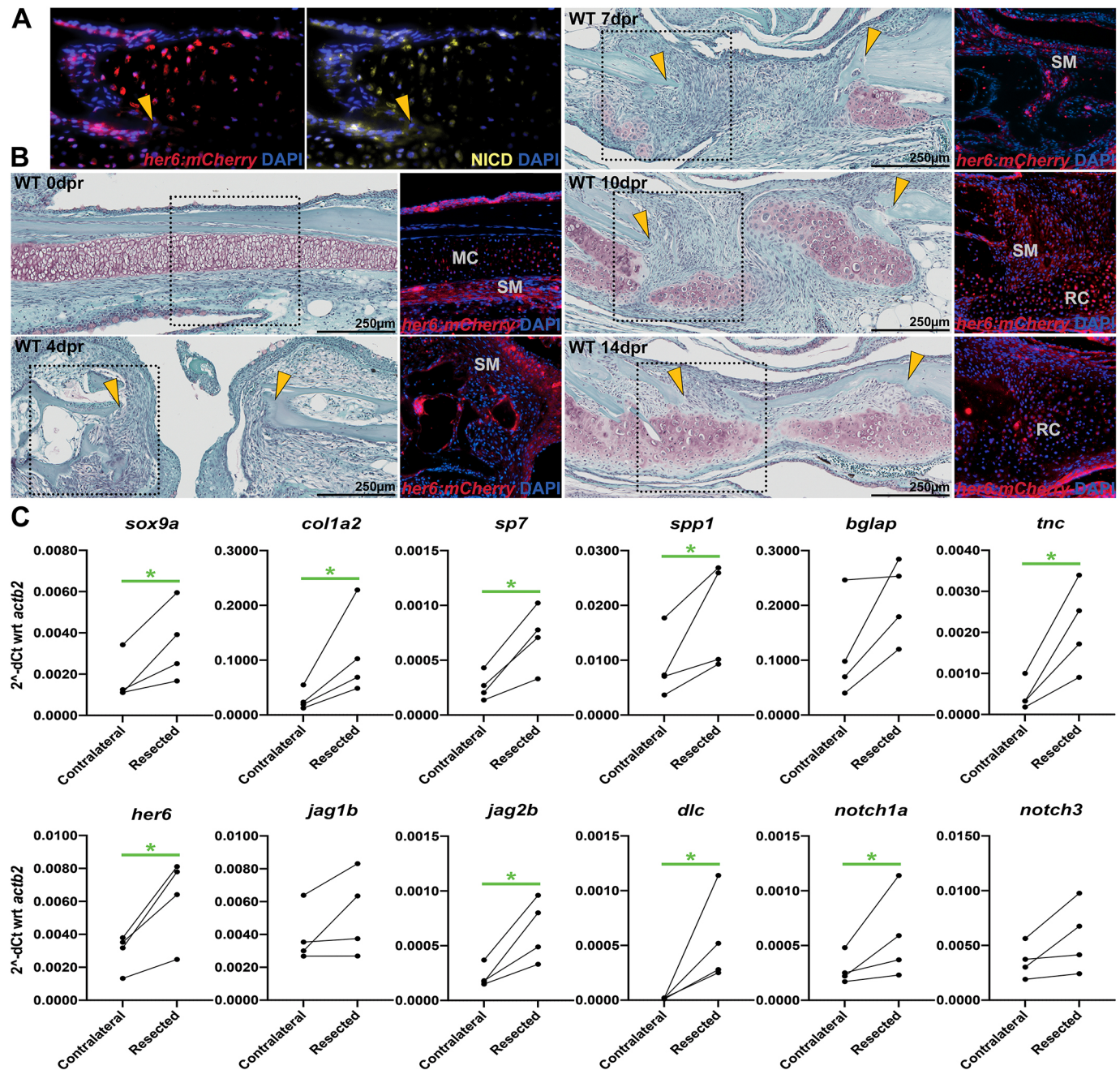


Fig. 1. Notch signaling is active in the regenerating mandible callus. (A) IHC of mCherry and NICD in a 10 dpr wild-type callus demonstrates colocalization of the *her6:mCherry* transgene with native NICD. (B) Safranin O staining (left column) and mCherry IHC (right column) from 0–32 dpr reveal spatiotemporal context of Notch signaling during mandible regeneration. Dotted boxes in Safranin O images represent approximate source locations and scale of IHC images from adjacent slides. MC, Meckel's chondrocytes; RC, repair chondroblasts; SM, stromal/mesenchymal cells. Yellow arrowheads indicate approximate surgical margins. (C) At 10 dpr, broad upregulation of osteochondral and Notch signaling-associated genes was observed by qPCR within the callus. Each point represents a different pool of least 11 animals, and solid lines connect paired resected versus contralateral (unresected) tissues. * $P < 0.05$ (ratio-paired, two-tailed *t*-tests).

reduced callus cellularity was observed in the DBZ group, and the robust *her6:mCherry*⁺ chondroid callus noted in the DMSO group (as well as in wild-type animals in Fig. 1B) was absent. In the DBZ group, *her6:mCherry*⁺ cells were only present in the skin and Meckel's chondrocytes at 18 dpr. Between 18 and 32 dpr, the cartilaginous callus in the DMSO group had typically resolved into bone, with no remaining cartilage. There was limited bone formation in the DBZ group, and delayed *her6:mCherry*⁺ activity was visible on bone surfaces and adjacent mesenchyme at 32 dpr in the DBZ group.

To determine whether arrest of callus formation was caused by defects in proliferation and/or apoptosis, 5-bromo-2'-deoxyuridine (BrdU) and caspase-3 IHC was performed at 6 dpr (Fig. 3C). There were fewer BrdU⁺ proliferating cells in the DBZ group ($P = 0.021$), whereas apoptosis was not affected. Gene expression analysis of DBZ versus DMSO animals at 10 dpr confirmed transcriptional downregulation of *her6* ($69.0 \pm 13.9\%$), as well as a broad profile of osteochondral genes (Fig. 3D, Fig. S3). Representative genes and their percentage reductions include: *sox9a* down $19.7 \pm 8.2\%$ ($P = 0.004$), *col1a2* down $77.8 \pm 4.3\%$ ($P < 0.001$), *sp7* down

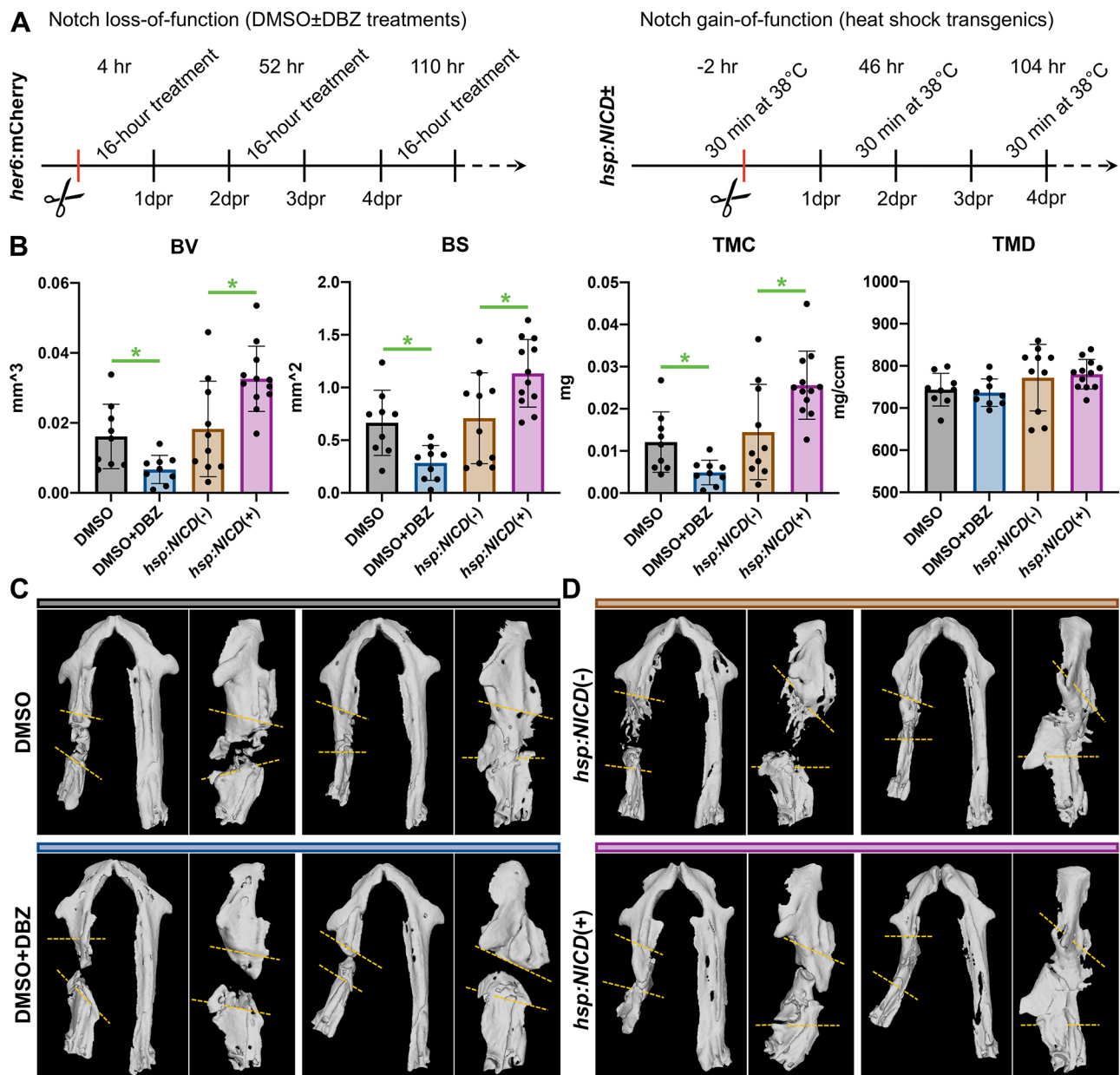


Fig. 2. Regenerate bone quantity scales with post-operative Notch signaling dose. (A) Complementary approaches were used to assess the role of Notch signaling in mandible regeneration during the initial post-operative period. (B) μ CT analyses at 32 dpr demonstrate reduced bone formation following DBZ treatment and enhanced bone formation with *hsp:NICD*. Notch signaling levels correlate with bone quantity (BV, BS, TMC) but not density (TMD). The four groups represent 9, 9, 10 and 12 animals, from left to right. Each data point represents an individual fish, with bars depicting mean \pm s.d. * $P < 0.05$ (two-tailed t -tests with Welch's correction). (C, D) Two representative μ CT surface renderings are shown for each group to illustrate range, in two orientations offset by 90°: supine, and lateral recumbent with the intact side digitally removed for clarity. Approximate surgical margins are depicted with yellow dashed lines; actual injury margins were carefully delineated slice-by-slice during μ CT analysis.

66.0 \pm 12.4% ($P = 0.001$), among others. The dominant Notch ligand, *jag1b*, was downregulated 68.5 \pm 3.4% ($P = 0.001$; Fig. S3). Thus, a broad spectrum of callus osteochondral markers and extracellular products were downregulated in DBZ-treated animals.

Fluorescence *in situ* hybridization (ISH) was used to assess the differentiation state of the hybrid cartilage-bone callus, using *col2a1a* and *coll1a1a* as early markers of cartilage and bone, respectively. These genes are co-expressed in repair chondroblasts (Paul et al., 2016), and labeled the mid-callus mesenchyme of the DMSO group. DBZ treatment decreased expression of both markers relative to DMSO, and notably increased the *col2a1a/coll1a1a* ratio ($P = 0.028$) (Fig. 3E). We conclude that Notch signaling within a

narrow post-operative window is required for the proliferative expansion and subsequent osteogenic conversion of the regenerative mandible callus. Failure of these processes as a result of Notch inhibition leads to atrophic non-union.

Conditional overactivation of Notch signaling enhances mandibular bone regeneration

The cellular basis of enhanced healing in Notch 1a transgenic animals was then assessed. Samples from heat-shocked *hsp:NICD⁺* and *hsp:NICD(-)* animals were first analyzed histologically by Safranin O staining and Sox9a, NICD and PCNA IHC at 6, 8, 10 and 32 dpr (Fig. 4A, B, Fig. S4A, B, Fig. S5). Although the initial response from

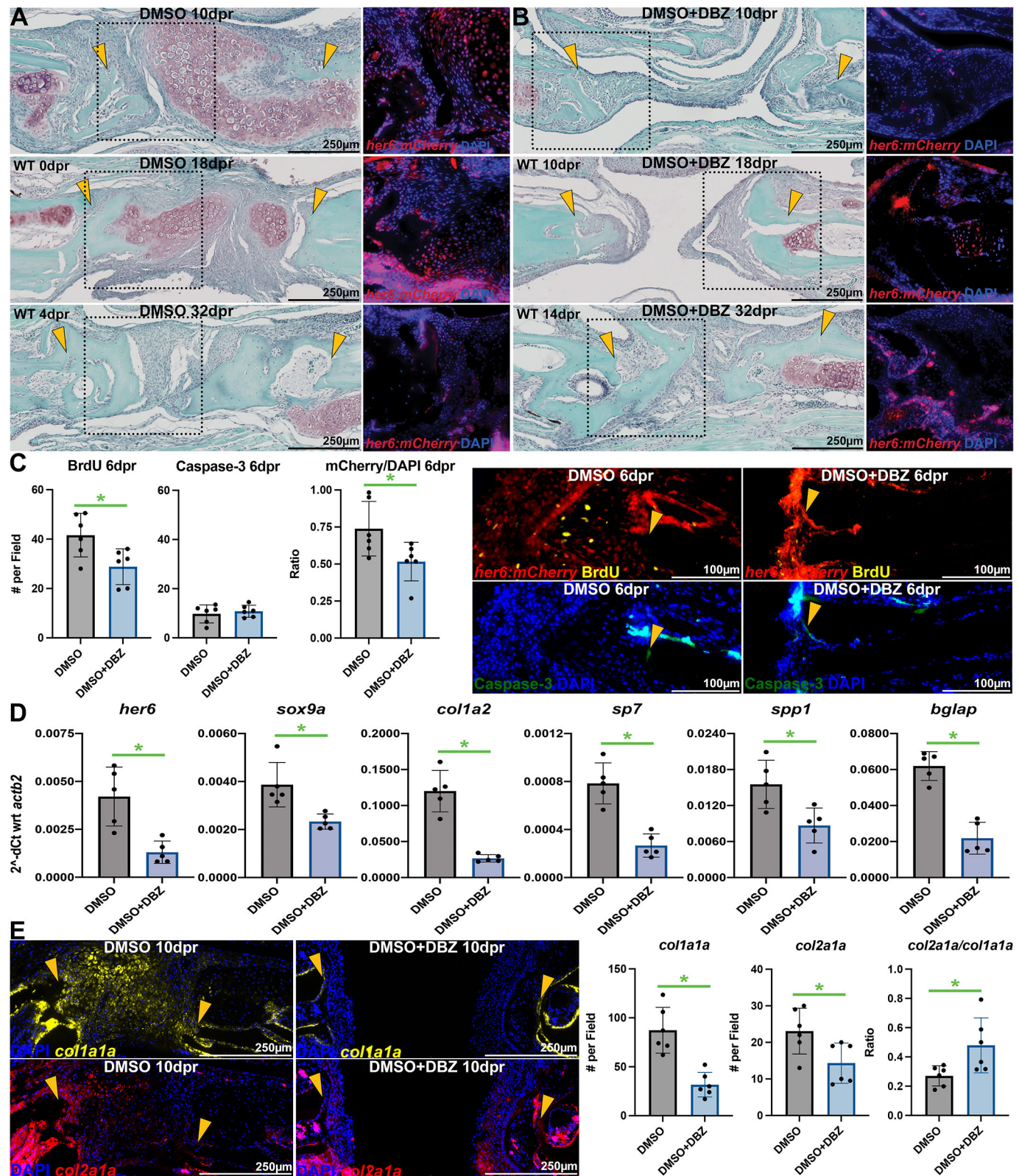


Fig. 3. Inhibition of Notch signaling represses osteochondral callus formation. (A,B) Safranin O staining (left column) and mCherry IHC (right column) from *her6:mCherry* reporter zebrafish at 10–32 dpr reveal inhibition of initial callus formation and Notch signaling following three sessions of post-operative DBZ treatment (as in Fig. 2A). Dotted boxes in Safranin O images represent approximate source locations and scale of IHC images from adjacent slides. Yellow arrowheads indicate approximate surgical margins. (C) At 6 dpr, DBZ treatment decreased proliferation (as measured by BrdU staining) of mCherry⁺ cells at the injury margins, whereas apoptosis (measured by caspase-3 IHC) was not changed ($n=6$ per group). Representative images are shown on the right. Yellow arrowheads indicate approximate surgical margins. (D) At 10 dpr, 5 days following the conclusion of DBZ treatment, lasting alterations in callus osteochondral gene expression were observed. Each point represents a pool of least 11 animals ($n=5$ pools in each group). (E) ISH for *col1a1a* and *col2a1a* reveals fewer callus cells and increased *col2a1a/col1a1a* ratio following DBZ treatment ($n=6$ per group). Each data point represents an individual fish, except for qPCR data, for which each point represents a different pool. Bars depict mean \pm s.d. * $P<0.05$ (two-tailed t -tests with Welch's correction).

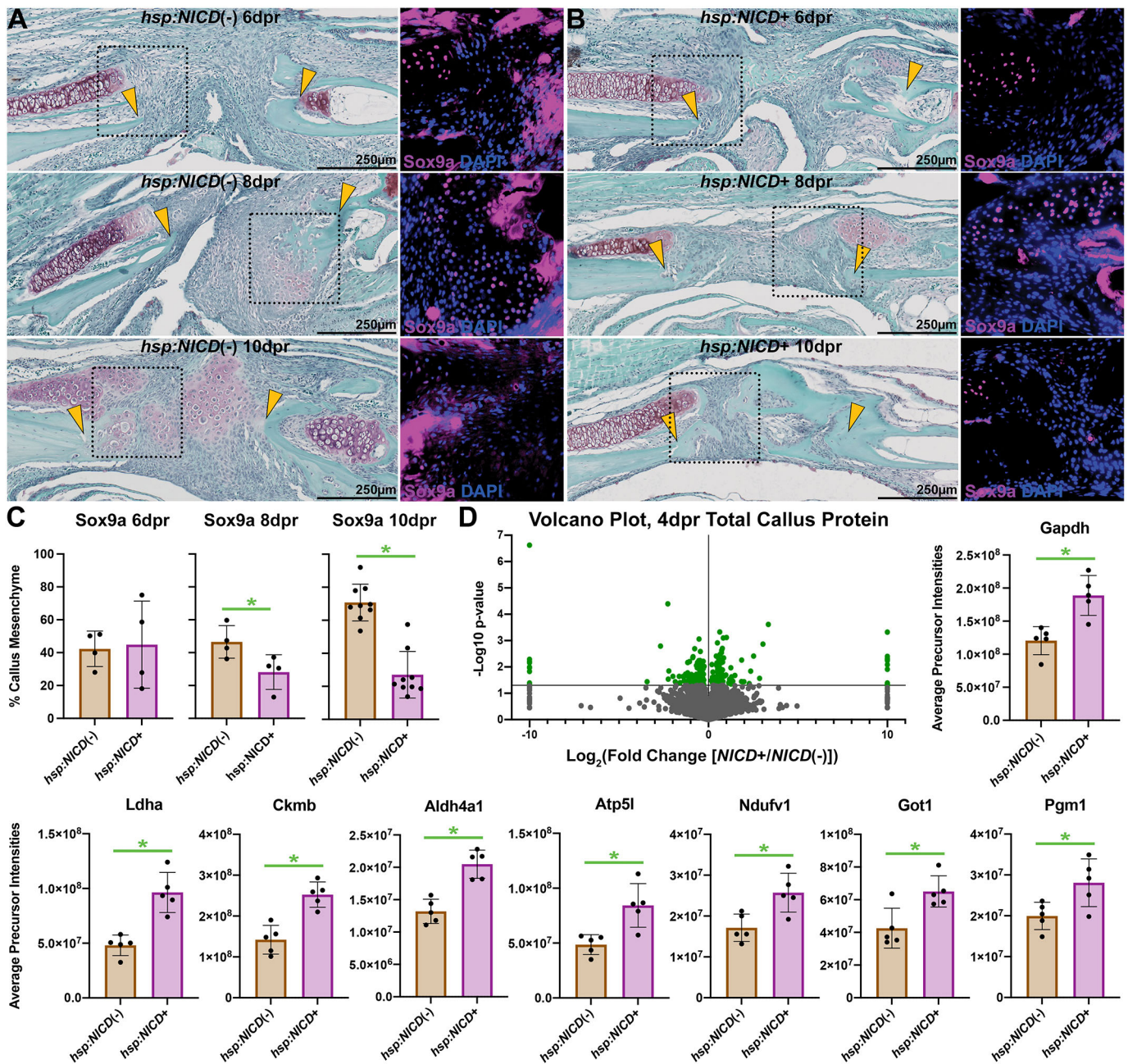


Fig. 4. Overactivation of Notch signaling results in direct, accelerated bone regeneration. (A,B) Safranin O staining (left column) and Sox9a IHC (right column) show a marked trend of decreased cartilage and increased bone from 6–10 dpi in *hsp:NICD*⁺ animals relative to heat-shocked *hsp:NICD*⁻ sibling controls (treated as in Fig. 2A). Dotted boxes in Safranin O images represent approximate source locations and scale of IHC images from adjacent slides. Yellow arrowheads indicate approximate surgical margins. (C) Quantification of Sox9a IHC reveals divergent trajectories of Sox9a positivity based on Notch signaling dose. Percentage is calculated by the number of Sox9a⁺ cells over the total DAPI count per field ($n=4$ per group at 6 and 8 dpi; $n=9$ per group at 10 dpi). (D) A volcano plot depicts dysregulated proteins between the *hsp:NICD*⁺ and *hsp:NICD*⁻ mandible calluses at 4 dpi. Major and reproducible changes to proteins with known functions in metabolism and osteogenesis were detected, including numerous enzymes associated with aerobic glycolysis ($n=4$ per group). Green dots in the volcano plot represent significantly dysregulated proteins. In bar graphs, each data point represents an individual fish, with bars depicting mean \pm s.d. * $P<0.05$ (two-tailed t -tests with Welch's correction).

the injury margin involved Sox9a⁺ cells, from 8 to 10 dpi these cells exhibited divergent differentiation trajectories. By 10 dpi, there was less Safranin O⁺ cartilage in the *hsp:NICD*⁺ group, and the percentage of mesenchymal cells retaining Sox9a positivity was $70.8 \pm 11.1\%$ in *hsp:NICD*⁻ animals versus $27.0 \pm 14.1\%$ in their *hsp:NICD*⁺ siblings ($P<0.001$) (Fig. 4C). PCNA IHC also showed a temporal shift in overall proliferation, peaking at 6 dpi rather than 10 dpi

(Fig. S5). Furthermore, osteoclast histomorphometry was assessed by tartrate-resistant acid phosphatase (TRAP) staining, and the absence of a phenotype supports an osteoblast lineage-specific phenotype in the *hsp:NICD*⁺ group (Fig. S4D). Thus, overactivation of NICD drives callus mesenchymal cells to a particularly osteogenic fate, with evidence of increased proliferation early in the injury response followed by accelerated callus ossification.

Proteomic analysis was performed on total callus lysate from 4 dpr heat-shocked *hsp:NICD*⁺ and *hsp:NICD*(−) samples to capture changes in protein levels within hours of the final heat shock. In total, 196 proteins were dysregulated by NICD overexpression (Fig. 4D); the three most highly enriched gene ontology (GO) biological process terms were ‘aspartate metabolic process’, ‘dicarboxylic acid metabolic process’ and ‘glucose metabolic process’. Closer review of significantly upregulated proteins revealed a metabolic landscape characteristic of aerobic glycolysis. Described as analogous to the Warburg effect, this involves a shift from oxidative phosphorylation to rapid but inefficient cytoplasmic glycolysis regardless of oxygen tension (Esen and Long, 2014). Dysregulated proteins in the NICD group (Fig. 4D) included a 2.9-fold increase in L-lactate dehydrogenase A chain (*Ldha*; *P*<0.001), a 1.8-fold increase in creatine kinase (*Ckmb*; *P*<0.001), a 1.5-fold increase in aldehyde dehydrogenase multifunctional fusion protein (*Aldh4a1*; *P*<0.001), a 1.7-fold increase in ATP synthase subunit (*Atp5l*; *P*=0.007), a 1.5-fold increase in NADH dehydrogenase (ubiquinone) flavoprotein 1, mitochondrial (*Ndufv1*; *P*=0.011), a 1.5-fold increase in aspartate aminotransferase (*Got1*; *P*=0.012) and a 1.4-fold increase in phosphoglucomutase 1 (*Pgm1*; *P*=0.027), among many related changes. We conclude that Notch overexpression results in upregulation of enzymes for aerobic glycolysis, increasing energy availability for accelerated bone regeneration (Lee et al., 2017; Slaninova et al., 2016; Lu et al., 2013; Shyh-Chang et al., 2013). Together with other hits having known functions in bone (Fig. S4C), these proteomic data encourage further investigation of the molecular basis of rapid regenerative ossification.

Insights into the role of Notch signaling in fracture healing

We posit a nuanced role for Notch signaling in multiple phases of regeneration (Youngstrom and Hankenson, 2019). During mandible regeneration in zebrafish, we report that regenerate bone quantity scales with Notch signaling owing to its positive regulatory roles during both callus proliferation and osteoblast differentiation/anabolism.

Recent work in the field of fracture healing has highlighted remarkable phenotypic complexity of cells involved in bone repair (Matthews et al., 2021; Wong et al., 2020). Our colleagues recently reported that conditional overexpression of NICD using *ACTA2-Cre*^{ERT2} results in accelerated ossification of fracture cartilage in mice (Novak et al., 2020). In addition to validating the common Notch requirement between mice and zebrafish, we expand on this study by showing that initial callus size is regulated by Notch, and also revealing significant, lasting improvements in mandibular bone regeneration from activation of Notch signaling within a narrow postoperative window. Together with our previous work (Paul et al., 2016), we hypothesize an iterative role of Notch-Hedgehog-Notch signaling in osteochondral repair.

Our approach to conditional overexpression of NICD was temporally restricted relative to experiments by Grotek et al. that resulted in lineage arrest of dedifferentiated caudal fin osteoblasts with sustained post-operative activation of *hsp:NICD* (Grotek et al., 2013). The developmental and regenerative programs of fin rays and the mandible are significantly divergent, and the initial mandible callus is formed by *Sox9a*⁺ cells. Because zebrafish cartilage cells show not only significant plasticity during regeneration, but also contribute to developmental osteoblasts and adipocytes (Giovannone et al., 2019), our work specifically implicates Notch signaling in both recruitment and ossification of *Sox9a*⁺ hybrid callus cells. Although we favor a model in which Notch signaling causes accelerated

ossification of cartilage, an alternative explanation is that Notch signaling selects for a subpopulation of particularly osteogenic progenitor cells. The stage-specific role of Notch signaling, and its intersection with other pathways that regulate osteochondral repair, will likely be fruitful areas of future investigation.

Conclusions

Zebrafish provide a useful model for understanding efficient mechanisms of skeletal repair. By way of molecular or genetic modulation of post-operative Notch signaling *in vivo*, we conclude that the extraordinary bone regeneration observed in the zebrafish craniofacial skeleton is contingent on functional Notch signaling. Furthermore, conditional genetic overactivation of this pathway enhances bone accrual by control of proliferation, differentiation and metabolism in osteochondral lineages. Continued investigation of this phenotype could lead to discoveries applicable to mammalian regenerative medicine. Finally, owing to the similarities between mandible and long-bone healing (Wong et al., 2020), relatively high-throughput zebrafish surgical models have potential utility for screening fracture therapeutics *in vivo* at scale.

MATERIALS AND METHODS

Generation of *Tg(her6:mCherry)*^{sd64} reporter fish

Two PCR products forming a 7.4 kb fragment immediately upstream of the *her6* transcriptional start site were amplified from the bacmid DKEY-111K7 and sequentially sub-cloned into a Tol2 transgenesis vector (Kawakami, 2004) containing the mCherry coding sequence. This fragment contains four RBPjk/Notch-responsive elements based on the consensus sequence YGTGRGAAM. The following primers were used: SacII-*her6*-7.4kb-For, ATACCGCGGcactctgtttaaactcccc; NotI-*her6*-3kb-Rev, ATAGCGGCC-GCataagttggcggttcattccg; NotI-*her6*-3kb-for, ATAGCGGCCGcaatgaa-cgccaactatcc; Spel-*her6*-ATG-rev, AATACTAGTctctgggaagtatccttcg (lowercase letters represent target genomic sequence). The final construct was co-injected with mRNA encoding the Tol2 transposase into one-cell-stage embryos. Embryos that showed transient transgene expression were raised and mated to establish founders for this novel transgenic line.

Animals

In this study, 385 zebrafish (*Danio rerio*, laboratory strain AB) with a mean age of approximately 6 months were used with IACUC approval from the University of Connecticut Health Center. Experimental endpoints are reported in dpr. The following transgenic lines were used in this study: *Tg(her6:mCherry)*^{sd64}, *Tg(hsp70l:Gal4)*^{ka4} and *Tg(UAS:myc-Notch1a-intra)*^{ka3}; the latter two constitute a conditional transcriptional activator and effector pair (Scheer and Campos-Ortega, 1999). For simplification in the text, reporter animals are transcribed as *her6:mCherry*, and *hsp70l:Gal4*; *UAS:myc-Notch1a-intra* animals as *hsp:NICD*⁺. *her6:mCherry* animals were genotyped by native fluorescence, and *hsp:NICD*⁺ and *hsp:NICD*(−) animals were genotyped by tail biopsy using published primers (Barske et al., 2016).

her6:mCherry zebrafish were used to perform initial histological assessment of regeneration, and for experiments involving histology of DBZ-treated animals *hsp:NICD*⁺ and *hsp:NICD*(−) zebrafish were used for conditional genetic overactivation of Notch signaling. Wild-type zebrafish on the same AB9 background were used for all other experiments. Animals of both sexes were used indiscriminately, and all transgenic animals had grossly normal phenotypes. Fish were housed in a custom facility with automated environmental controls (Aquaneering, San Diego, CA, USA). Euthanasia was performed by submersion in 400 mg/l tricaine methanesulfonate (MS-222; Syndel) in system water, which was then moved over ice.

Treatments

DBZ (CAS 209984-56-5; Syncom) is a γ -secretase inhibitor used to pharmacologically inhibit cleavage of the active intracellular domain of Notch receptors. To treat fish with 20 μ M DBZ, 400 μ l of 50 mM DBZ stock in DMSO (BP231; Fisher BioReagents) was added per liter of system water

(final DMSO concentration 0.1%). DMSO without DBZ was used as a vehicle negative control. Initial DBZ treatments were applied in three 16-h intervals, 48 h apart, beginning 4 h after mandibulectomy. Follow-up DBZ treatment windows were single 48-h exposures at a range of times between 0 and 5 dpr.

To overactivate Notch signaling, *hsp:NICD⁺* and *hsp:NICD(-)* animals were treated with heat, causing transient systemic overexpression of the (activated) NICD by heat shock-mediated Gal4/UAS transgenics. Controls were *hsp⁺* animals lacking the *NICD* transgene and heat-treated in parallel. Animals were transferred to 38°C system water for three 30-min intervals, 48 h apart, beginning 2 h prior to mandibulectomy.

A cohort of DMSO±DBZ fish were immersed in system water containing 4.5 mg/ml BrdU (5002, Sigma-Aldrich) for 1 h and washed with a continuous flow of system water for 30 min prior to euthanasia.

Histology

Samples were fixed in 10% neutral buffered formalin and processed for histology. Fish were decapitated, decalcified in 20% EDTA, pH 7.4, dehydrated in stepped solutions of ethanol/xylenes, and embedded in paraffin. Blocks were sectioned at 5 µm using a microtome, and deparaffinized prior to staining. All histological images are representative of at least *n*=5 biological replicates per group. Approximate surgical margins are marked with yellow arrows.

For cartilage Safranin O histology, nuclei were stained using modified Weigert's iron hematoxylin differentiated in acid-ethanol, 0.02% Fast Green was used as a counterstain, and 1% Safranin O was used to stain the proteoglycan-rich extracellular matrix of cartilage. Slides were mounted in toluene media. Representative sections were imaged using an Axio Scan.Z1 slide scanner (Zeiss Microscopy). Dotted squares in Safranin O images represent approximate source locations of IHC insets from adjacent slides.

For IHC (indirect immunofluorescence), slides were subjected to membrane permeabilization in acetone and antigen retrieval in citrate, pH 6.0, or commercial reagent (550524; BD Biosciences) in a pressure cooker for 3 min. Two percent goat serum with 1% DMSO and phosphate-buffered saline with 0.05% Tween-20 (BP337; Fisher BioReagents) or commercial buffer (37580, Thermo Fisher Scientific) was used for blocking. Novus NBP2-25158 chicken anti-mCherry antibody (Centennial) was used as a primary antibody for *her6:mCherry* fish at 1:250 and incubated at 4°C overnight. Abcam AB175477 goat anti-chicken Alexa Fluor 568 was used as a secondary antibody at 1:500 at 4°C for 1 h. Additional antibodies used were: GeneTex GTX48504 goat anti-Notch1a ICD (recognizing amino acids 2314-2327, QNMAMPQHQNHSHH, near the C-terminus; NP_571516.1), Sigma-Aldrich MoBU-1 mouse anti-BrdU, BD Biosciences 559565 rabbit anti-caspase-3, GeneTex GTX128370 rabbit anti-Sox9a, Invitrogen 133900 mouse anti-PCNA, and Invitrogen secondary antibodies A32849, A11011, A11001, A11008 and A32787. Slides were mounted with DAPI glycerol-based media (P36966, Molecular Probes). Images were acquired on a Leica DMI6000B fluorescence microscope. Antibody lot numbers are reported in Table S2. Quantification was performed by single-channel color thresholding and particle counting in ImageJ, manually confirmed. Numbers are reported per 0.144 mm² field. *her6:mCherry(-)* animals and IHC slides lacking primary antibodies were negative controls.

For fluorescence ISH, *coll1a1* and *col2a1a* transcripts were detected using a previously published protocol (Paul, et al., 2016). Briefly, pCR-Blunt II-TOPO plasmids with kanamycin resistance-containing blunt probe insertions were propagated in DH5α cells (18265017, Invitrogen). Plasmid DNA was extracted, linearized and purified (Thermo Fisher Scientific K0502, K0691). DIG/DNP-labeled riboprobes (PerkinElmer NEL555001EA; Roche 11277073910.) were transcribed, isolated and sequentially hybridized. Fluorescence was visualized following tyramide signal amplification (Perkin Elmer NEL747A001KT, NEF832001EA, NEL704A001KT, NEL705A001KT). Two fields per sample, one anterior and one posterior, were segmented for callus mesenchyme and counted in ImageJ.

TRAP histomorphometry

A commercial TRAP kit (387A, Sigma-Aldrich) was used to stain osteoclasts. Samples were coverslipped using aqueous media

(VectaMount AQ) and imaged within 24 h. Histomorphometry was performed in Osteomeasure7 (OsteoMetrics) using an Olympus BX53 with Wacom pen computer. A single mid-callus field was captured and analyzed for each specimen using a 20× objective. Parameters are reported per 0.26 mm² field.

qPCR

Immediately following euthanasia at 10 dpr, the injury site (callus), and for some experiments, matched contralateral mandible tissue, was microdissected under a Leica M165FC stereomicroscope; *n*=4 replicate pools per group of *n*=11-13 fish each were prepared in 1 ml of TRIzol (Thermo Fisher Scientific) at 4°C, and homogenized in a bead mill (Minily, Bertin Technologies) prior to storage at -80°C. Total RNA was isolated by standard AGPC extraction and purified by solid phase extraction (7326830, Bio-Rad Laboratories) with on-column DNase digestion. RNA was reverse-transcribed (RT; Bio-Rad, 1708840), and 80 ng of cDNA per reaction was run in at least duplicate in a Bio-Rad CFX96 Real-Time System using SYBR Green chemistry (Bio-Rad, 1725270). (-)RT sample templates served as negative controls.

Primer pairs (synthesized by Integrated DNA Technologies) were either identified from the literature (Casadei et al., 2011; Lin et al., 2013; Wiweger et al., 2014) or custom-designed in NCBI Primer-BLAST to span exons (Table S1). Primers were validated by melt curve analysis and gel electrophoresis of qPCR products. Expression levels are reported as 2^{-dCt} with respect to the housekeeping gene *actb2*, which allows reference-free interpretation (Youngstrom et al., 2020). Raw dCt values were used for statistical analysis.

µCT

Samples were imaged on a Scanco µCT40 specimen scanner at 12 µm³ resolution at the following settings: 55 k Vp, 145 µA, 300 ms integration time, 500 projections/180°. Bone within regenerating mandibular defects was quantified by slice-by-slice manual segmentation of all new bone within and adjacent to the injury margins, which were detected by radiodensity and with respect to anatomical landmarks. The first precaudal/thoracic (T1) vertebra of each fish was also analyzed: the hourglass-shaped vertebral bodies were manually segmented, slice-by-slice, from all processes (Suniaga et al., 2018). BV, BS, TMC and TMD are reported from these defined volumes of interest, with a lower threshold of 450 mgHA/ccm. All µCT data represent a minimum of *n*=8 biological replicates per group.

Proteomics

Total protein was isolated from *hsp:NICD⁺* and *hsp:NICD(-)* animals (*n*=5 per group) at 4 dpr. Microdissected callus tissue was lysed with commercial protein extraction reagent (M-PER 78501, Thermo Fisher Scientific) in the presence of protease inhibitors, ultrasonicated, and quantified by BCA assay (Pierce Rapid Gold, Thermo Fisher Scientific). 200 µg aliquots were analyzed by an UltiMate 3000 RSLCnano ultra-high performance liquid chromatography system coupled to a Q Exactive HF tandem mass spectrometer (UPLC-MS/MS; Thermo Fisher Scientific). Raw data were searched against the *Danio rerio* UniProt reference proteome (UP000000437) using MaxQuant v1.6.10.43 (Max Planck Institute of Biochemistry). Data visualization and statistical analysis was performed in Scaffold Q+S v5.0.0 (Proteome Software). GO terms were generated using an unranked list of enriched (*P*<0.05) targets as foreground against the entire identified protein list as background via the Gene Ontology enrichment tool (GO) (Eden et al., 2009). Full experimental details are included in supplementary Materials and Methods, and raw data are available via ProteomeXchange with identifier PXD027280.

Statistics

Prism 9 (GraphPad Software) was used for statistical analysis and graph production. Wild-type 10 dpr qPCR comparisons between matched resected and contralateral mandibles were analyzed using ratio-paired, two-tailed *t*-tests of raw dCt values. All µCT, qPCR, histologic and proteomic data were analyzed using unpaired, two-tailed *t*-tests with Welch's correction. Each experimental group (DBZ or *hsp:NICD⁺*) was only compared with its

associated control. Statistical significance for all experiments was set at $P \leq 0.05$, graphically depicted by asterisks within figures.

Acknowledgements

Megan Matsutani, Claire E. Arata, Sanja Novak and Emily A. Gardner provided valuable logistical and technical assistance. We also thank Archana Sanjay, Ivo Kalajzic and Parker K. Acevedo for helpful discussions.

Competing interests

The authors declare no competing or financial interests.

Author contributions

Conceptualization: K.D.H., J.G.C., D.W.Y.; Methodology: J.M.K., J.L.S., J.Y.B., D.T., J.G.C., D.W.Y.; Software: R.R., J.L.B., D.W.Y.; Validation: J.M.K., D.G., R.R., J.G.C., D.W.Y.; Formal analysis: J.M.K., J.L.B., D.W.Y.; Investigation: J.M.K., D.G., D.W.Y.; Resources: J.L.B., I.L.M., D.T., K.D.H., J.G.C., D.W.Y.; Data curation: J.M.K., R.R., J.L.B., D.W.Y.; Writing - original draft: D.W.Y.; Writing - review & editing: J.M.K., D.G., R.R., J.L.B., I.L.M., J.L.S., J.Y.B., D.T., K.D.H., J.G.C., D.W.Y.; Visualization: D.W.Y.; Supervision: I.L.M., K.D.H., J.G.C., D.W.Y.; Project administration: D.W.Y.; Funding acquisition: D.T., K.D.H., J.G.C., D.W.Y.

Funding

This work was funded in part by an Orthopaedic Research Society Collaborative Exchange Grant (D.W.Y.), the National Institutes of Health (F32 DE026346 to D.W.Y.; R01 AR069700 and R35 DE027550 to J.G.C.; R01 DK074482 to D.T.; R01 DE030660 and R01 AR066028 to K.D.H.) and the U.S. Department of Defense Congressionally Directed Medical Research Programs (W81XWH-15-1-0689 to K.D.H.). Deposited in PMC for release after 12 months.

Data availability

Proteomics data have been deposited in the ProteomeXchange database under accession number PXD027280.

Peer review history

The peer review history is available online at <https://journals.biologists.com/dev/article-lookup/doi/10.1242/dev.199995>.

References

- Alyahya, A. and Swennen, G. R. J. (2019). Bone grafting in orthognathic surgery: a systematic review. *Int. J. Oral Maxillofac. Surg.* **48**, 322-331. doi:10.1016/j.ijom.2018.08.014
- Bales, C. B., Kamath, B. M., Munoz, P. S., Nguyen, A., Piccoli, D. A., Spinner, N. B., Horn, D., Shults, J., Leonard, M. B., Grimberg, A. et al. (2010). Pathologic lower extremity fractures in children with Alagille syndrome. *J. Pediatr. Gastroenterol. Nutr.* **51**, 66-70. doi:10.1097/MPG.0b013e3181cb9629
- Barske, L., Askary, A., Zuniga, E., Balczerski, B., Bump, P., Nichols, J. T. and Crump, J. G. (2016). Competition between Jagged-Notch and Endothelin1 signaling selectively restricts cartilage formation in the zebrafish upper face. *PLoS Genet.* **12**, e1005967. doi:10.1371/journal.pgen.1005967
- Bergen, D. J. M., Kague, E. and Hammond, C. L. (2019). Zebrafish as an emerging model for osteoporosis: a primary testing platform for screening new osteo-active compounds. *Front. Endocrinol.* **10**, 6. doi:10.3389/fendo.2019.00006
- Brousseau, P. M. A. (1789). Memoir on the regeneration of certain parts of the bodies of fishes. *The Literary Magazine and British Review* **3**, 111-113. doi:10.5962/bhl.title.5761
- Busse, B., Galloway, J. L., Gray, R. S., Harris, M. P. and Kwon, R. Y. (2020). Zebrafish: an emerging model for orthopedic research. *J. Orthop. Res.* **38**, 925-936. doi:10.1002/jor.24539
- Casadei, R., Pelleri, M. C., Vitale, L., Facchin, F., Lenzi, L., Canaider, S., Strippoli, P. and Frabetti, F. (2011). Identification of housekeeping genes suitable for gene expression analysis in the zebrafish. *Gene Expr. Patterns* **11**, 271-276. doi:10.1016/j.gexp.2011.01.003
- Eden, E., Navon, R., Steinfeld, I., Lipson, D. and Yakhini, Z. (2009). GOrrilla: a tool for discovery and visualization of enriched GO terms in ranked gene lists. *BMC Bioinformatics* **10**, 48. doi:10.1186/1471-2105-10-48
- Esen, E. and Long, F. (2014). Aerobic glycolysis in osteoblasts. *Curr. Osteoporos Rep.* **12**, 433-438. doi:10.1007/s11914-014-0235-y
- Geurtzen, K., Knopf, F., Wehner, D., Huitema, L. F. A., Schulte-Merker, S. and Weidinger, G. (2014). Mature osteoblasts dedifferentiate in response to traumatic bone injury in the zebrafish fin and skull. *Development* **141**, 2225-2234. doi:10.1242/dev.105817
- Giovannone, D., Paul, S., Schindler, S., Arata, C., Farmer, D. T., Patel, P., Smeeton, J. and Crump, J. G. (2019). Programmed conversion of hypertrophic chondrocytes into osteoblasts and marrow adipocytes within zebrafish bones. *eLife* **8**, e42736. doi:10.7554/eLife.42736
- Grotek, B., Wehner, D. and Weidinger, G. (2013). Notch signaling coordinates cellular proliferation with differentiation during zebrafish fin regeneration. *Development* **140**, 1412-1423. doi:10.1242/dev.087452
- Hill, C. R., Yuasa, M., Schoenecker, J. and Goudy, S. L. (2014). Jagged1 is essential for osteoblast development during maxillary ossification. *Bone* **62**, 10-21. doi:10.1016/j.bone.2014.01.019
- Hoff, A. O., Toth, B. B., Altundag, K., Johnson, M. M., Warneke, C. L., Hu, M., Nooka, A., Sayegh, G., Guarneri, V., Desrouleaux, K. et al. (2008). Frequency and risk factors associated with osteonecrosis of the jaw in cancer patients treated with intravenous bisphosphonates. *J. Bone Miner. Res.* **23**, 826-836. doi:10.1359/jbmr.080205
- Howe, K., Clark, M. D., Torroja, C. F., Torrance, J., Berthelot, C., Muffato, M., Collins, J. E., Humphray, S., McLaren, K., Matthews, L. et al. (2013). The zebrafish reference genome sequence and its relationship to the human genome. *Nature* **496**, 498-503. doi:10.1038/nature12111
- Humphreys, R., Zheng, W., Prince, L. S., Qu, X., Brown, C., Loomes, K., Huppert, S. S., Baldwin, S. and Goudy, S. (2012). Cranial neural crest ablation of Jagged1 recapitulates the craniofacial phenotype of Alagille syndrome patients. *Hum. Mol. Genet.* **21**, 1374-1383. doi:10.1093/hmg/ddr575
- Kamalakar, A., McKinney, J. M., Duron, D. S., Amanso, A. M., Ballestas, S. A., Drissi, H., Willett, N. J., Bhattaram, P., Garcia, A. J. and Wood, L. B. (2021). Jagged1 stimulates cranial neural crest cell osteoblast commitment pathways and bone regeneration independent of canonical Notch signaling. *Bone* **143**, 115657. doi:10.1016/j.bone.2020.115657
- Kametani, Y., Chi, N. C., Stainier, D. Y. R. and Takada, S. (2015). Notch signaling regulates venous arterialization during zebrafish fin regeneration. *Genes Cells Dev.* **427-438**. doi:10.1111/gtc.12234
- Kawakami, K. (2004). Transgenesis and gene trap methods in zebrafish by using the Tol2 transposable element. *Methods Cell Biol.* **77**, 201-222. doi:10.1016/S0091-679X(04)77011-9
- Khan, A. A., Morrison, A., Hanley, D. A., Felsenberg, D., McCauley, L. K., O'Ryan, F., Reid, I. R., Ruggiero, S. L., Taguchi, A., Tetradis, S. et al. (2015). Diagnosis and management of osteonecrosis of the jaw: a systematic review and international consensus. *J. Bone Miner. Res.* **30**, 3-23. doi:10.1002/jbmr.2405
- Kim, J. E., Broyles, J. M. and Sacks, J. M. (2013). Mandible reconstruction. *Eplasty* **13**, ic19.
- King, R. E., Scianna, J. M. and Petruzzelli, G. J. (2004). Mandible fracture patterns: A suburban trauma center experience. *Am. J. Otolaryngol.* **25**, 301-307. doi:10.1016/j.amjoto.2004.03.001
- Knopf, F., Hammond, C., Chekuru, A., Kurth, T., Hans, S., Weber, C. W., Mahatma, G., Fisher, S., Brand, M. and Schulte-Merker, S. (2011). Bone regenerates via dedifferentiation of osteoblasts in the zebrafish fin. *Dev. Cell* **20**, 713-724. doi:10.1016/j.devcel.2011.04.014
- Kuwahara, S. T., Serowoky, M. A., Vakhshori, V., Tripuraneni, N., Hegde, N. V., Lieberman, J. R., Crump, J. G. and Mariani, F. V. (2019). Sox9+ messenger cells orchestrate large-scale skeletal regeneration in the mammalian rib. *eLife* **8**, e40715. doi:10.7554/eLife.40715
- Lee, W.-C., Guntur, A. R., Long, F. and Rosen, C. J. (2017). Energy metabolism of the osteoblast: Implications for osteoporosis. *Endocr. Rev.* **38**, 255-266. doi:10.1210/er.2017-00064
- Li, L., Krantz, I. D., Deng, Y., Genin, A., Banta, A. B., Collins, C. C., Qi, M., Trask, B. J., Kuo, W. L., Cochran, J. et al. (1997). Alagille syndrome is caused by mutations in human Jagged1, which encodes a ligand for Notch1. *Nat. Genet.* **16**, 243-251. doi:10.1038/ng0797-243
- Lin, C.-Y., Huang, C.-C., Wang, W.-D., Hsiao, C.-D., Cheng, C.-F., Wu, Y.-T., Lu, Y.-F. and Hwang, S.-P. L. (2013). Low temperature mitigates cardia bifida in zebrafish embryos. *PLoS ONE* **8**, e69788. doi:10.1371/journal.pone.0069788
- Lu, C., Saless, N., Wang, X., Sinha, A., Decker, S., Kazakia, G., Hou, H., Williams, B., Swartz, H. M., Hunt, T. K. et al. (2013). The role of oxygen during fracture healing. *Bone* **52**, 220-229. doi:10.1016/j.bone.2012.09.037
- Marschall, J. S., Flint, R. L., Kushner, G. M. and Alpert, B. (2019). Management of mandibular osteomyelitis with segmental resection, nerve preservation, and immediate reconstruction. *J. Oral Maxillofac. Surg.* **77**, 1490-1504. doi:10.1016/j.joms.2019.01.036
- Matthews, B. G., Novak, S., Sbrana, F. V., Funnell, J. L., Cao, Y., Buckels, E. J., Grcevic, D. and Kalajzic, I. (2021). Heterogeneity of murine periosteum progenitors involved in fracture healing. *eLife* **10**, e58534. doi:10.7554/eLife.58534
- Novak, S., Roeder, E., Sinder, B. P., Adams, D. J., Siebel, C. W., Grcevic, D., Hankenson, K. D., Matthews, B. G. and Kalajzic, I. (2020). Modulation of Notch1 signaling regulates bone fracture healing. *J. Orthop. Res.* **38**, 2350-2361. doi:10.1002/jor.24650
- Oda, T., Elkahoun, A. G., Pike, B. L., Okajima, K., Krantz, I. D., Genin, A., Piccoli, D. A., Meltzer, P. S., Spinner, N. B. and Collins, F. S. (1997). Mutations in the human Jagged1 gene are responsible for Alagille syndrome. *Nat. Genet.* **16**, 235-242. doi:10.1038/ng0797-235
- Olsen, I. E., Ittenbach, R. F., Rovner, A. J., Leonard, M. B., Mulberg, A. E., Stallings, V. A., Piccoli, D. A. and Zemel, B. S. (2005). Deficits in size-adjusted bone mass in children with Alagille syndrome. *J. Pediatr. Gastroenterol. Nutr.* **40**, 76-82. doi:10.1097/00005176-200501000-00014
- Paul, S., Schindler, S., Giovannone, D., de Millo Terrazzani, A., Mariani, F. V. and Crump, J. G. (2016). Ihha induces hybrid cartilage-bone cells during

- zebrafish jawbone regeneration. *Development* **143**, 2066-2076. doi:10.1242/dev.131292
- Pfefferli, C. and Jaźwińska, A.** (2015). The art of fin regeneration in zebrafish. *Regeneration (Oxf)* **2**, 72-83. doi:10.1002/reg2.33
- Rogers, S. N., Devine, J., Lowe, D., Shokar, P., Brown, J. S. and Vaugman, E. D.** (2004). Longitudinal health-related quality of life after mandibular resection for oral cancer: A comparison between rim and segment. *Head Neck* **26**, 54-62. doi:10.1002/hed.10351
- Schebesta, M., Lien, C.-L., Engel, F. B. and Keating, M. T.** (2006). Transcriptional profiling of caudal fin regeneration in zebrafish. *ScientificWorldJournal* **6** Suppl. 1, 38-54. doi:10.1100/tsw.2006.326
- Scheer, N. and Campos-Ortega, J. A.** (1999). Use of the Gal4-UAS technique for targeted gene expression in the zebrafish. *Mech. Dev.* **80**, 153-158. doi:10.1016/S0925-4773(98)00209-3
- Schilling, T. F., Walker, C. and Kimmel, C. B.** (1996). The chinless mutation and neural crest cell interactions in zebrafish jaw development. *Development* **122**, 1417-1426. doi:10.1242/dev.122.5.1417
- Shah, J. P. and Gil, Z.** (2009). Current concepts in management of oral cancer—surgery. *Oral Oncol.* **45**, 394-401. doi:10.1016/j.oraloncology.2008.05.017
- Shyh-Chang, N., Daley, G. Q. and Cantley, L. C.** (2013). Stem cell metabolism in tissue development and aging. *Development* **140**, 2535-2547. doi:10.1242/dev.091777
- Singh, S. P., Holdway, J. E. and Poss, K. D.** (2012). Regeneration of amputated zebrafish fin rays from de novo osteoblasts. *Dev. Cell* **22**, 879-886. doi:10.1016/j.devcel.2012.03.006
- Slaninova, V., Krafčikova, M., Perez-Gomez, R., Steffal, P., Trantirek, L., Bray, S. J. and Krejci, A.** (2016). Notch stimulates growth by direct regulation of genes involved in the control of glycolysis and the tricarboxylic acid cycle. *Open Biol.* **6**, 150155. doi:10.1098/rsob.150155
- Snyder, H. T., Bilboul, M. J. and Pope, A. W.** (2005). Psychosocial adjustment in adolescents with craniofacial anomalies: A comparison of parent and self-reports. *Cleft Palate Craniofac. J.* **42**, 548-555. doi:10.1597/04-078r.1
- Suniaga, S., Rolvien, T., Vom Scheidt, A., Fiedler, I. A. K., Bale, H. A., Huisseune, A., Witten, P. E., Amling, M. and Busse, B.** (2018). Increased mechanical loading through controlled swimming exercise induces bone formation and mineralization in adult zebrafish. *Sci. Rep.* **8**, 3646. doi:10.1038/s41598-018-21776-1
- Vaca, E. E., Bellamy, J. L., Sinno, S. and Rodriguez, E. D.** (2018). Management of high-energy avulsive ballistic facial injury: A review of the literature and algorithmic approach. *Plast. Reconstr. Surg. Glob. Open* **6**, e1693. doi:10.1097/GOX.0000000000001693
- Wiweger, M. I., de Andrea, C. E., Scheepstra, K. W. F., Zhao, Z. and Hogendoorn, P. C. W.** (2014). Possible effects of EXT2 on mesenchymal differentiation—Lessons from the zebrafish. *Orphanet J. Rare Dis.* **9**, 1-11. doi:10.1186/1750-1172-9-35
- Wong, S. A., Hu, D. P., Slocum, J., Lam, C., Nguyen, M., Miclau, T., Marcucio, R. S. and Bahney, C. S.** (2020). Chondrocyte-to-osteoblast transformation in mandibular fracture repair. *J. Orthop. Res.* **39**, 1622-1632. doi:10.1002/jor.24904
- Youngstrom, D. W. and Hankenson, K. D.** (2019). Contextual regulation of skeletal physiology by Notch signaling. *Curr. Osteoporos Rep.* **17**, 217-225. doi:10.1007/s11914-019-00516-y
- Youngstrom, D. W., Dishowitz, M. I., Bales, C. B., Carr, E., Mutyaba, P. L., Kozloff, K. M., Shitaye, H., Hankenson, K. D. and Loomes, K. M.** (2016). Jagged1 expression by osteoblast-lineage cells regulates trabecular bone mass and periosteal expansion in mice. *Bone* **91**, 64-74. doi:10.1016/j.bone.2016.07.006
- Youngstrom, D. W., Senos, R., Zondervan, R. L., Brodeur, J. D., Lints, A. R., Young, D. R., Mitchell, T. L., Moore, M. E., Myers, M. H., Tseng, W.-J. et al.** (2017). Intraoperative delivery of the Notch ligand Jagged-1 regenerates appendicular and craniofacial bone defects. *NPJ Regen Med* **2**, 32. doi:10.1038/s41536-017-0037-9
- Youngstrom, D. W., Zondervan, R. L., Doucet, N. R., Acevedo, P. K., Sexton, H. E., Gardner, E. A., Anderson, J. S., Kushwaha, P., Little, H. C., Rodriguez, S. et al.** (2020). CTRP3 regulates endochondral ossification and bone remodeling during fracture healing. *J. Orthop. Res.* **38**, 996-1006. doi:10.1002/jor.24553

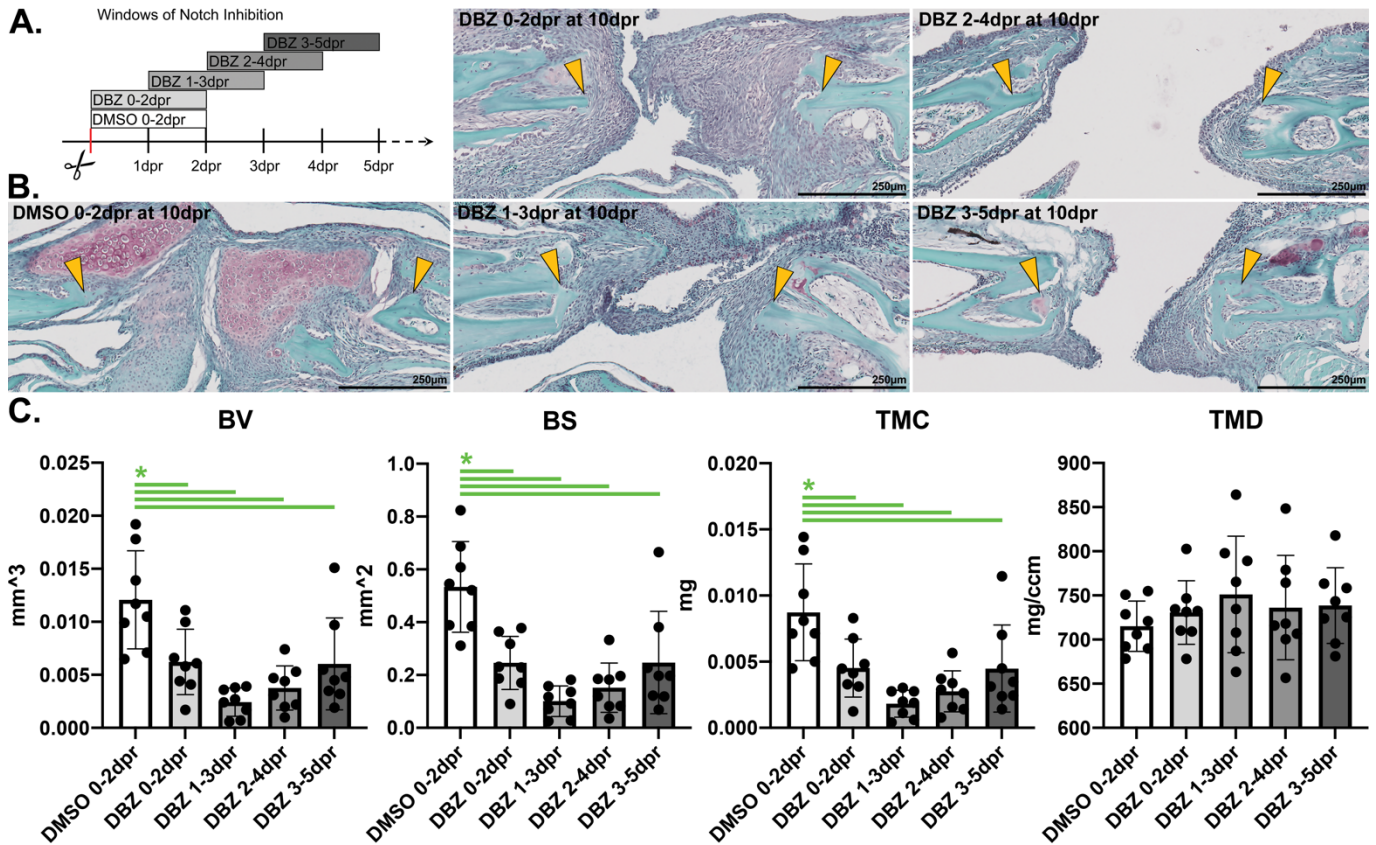


Fig. S1. Early Notch signaling is necessary for mandible regeneration. (A) A series of 48-hour DBZ treatments was used to identify the postoperative period most sensitive to Notch inhibition. (B) Stunted callus formation and an absence of cartilage was observed in all DBZ-treated groups by Safranin O histology, and 48-hour DBZ treatments conducted at 4 windows from 0-2 dpr to 3-5 dpr all result in soft tissue non-union. (C) Though DBZ windows were not sufficiently powered to reach statistical significance from each other via multiple comparisons, the 1-3 dpr period had the lowest mean regenerate bone at 32 dpr. Each graphed datapoint represents an individual fish (n=8 in each group), with bars depicting means and standard deviations. Green lines/asterisks represent statistical significance (p<0.05) using two-tailed t-tests with Welch's correction.

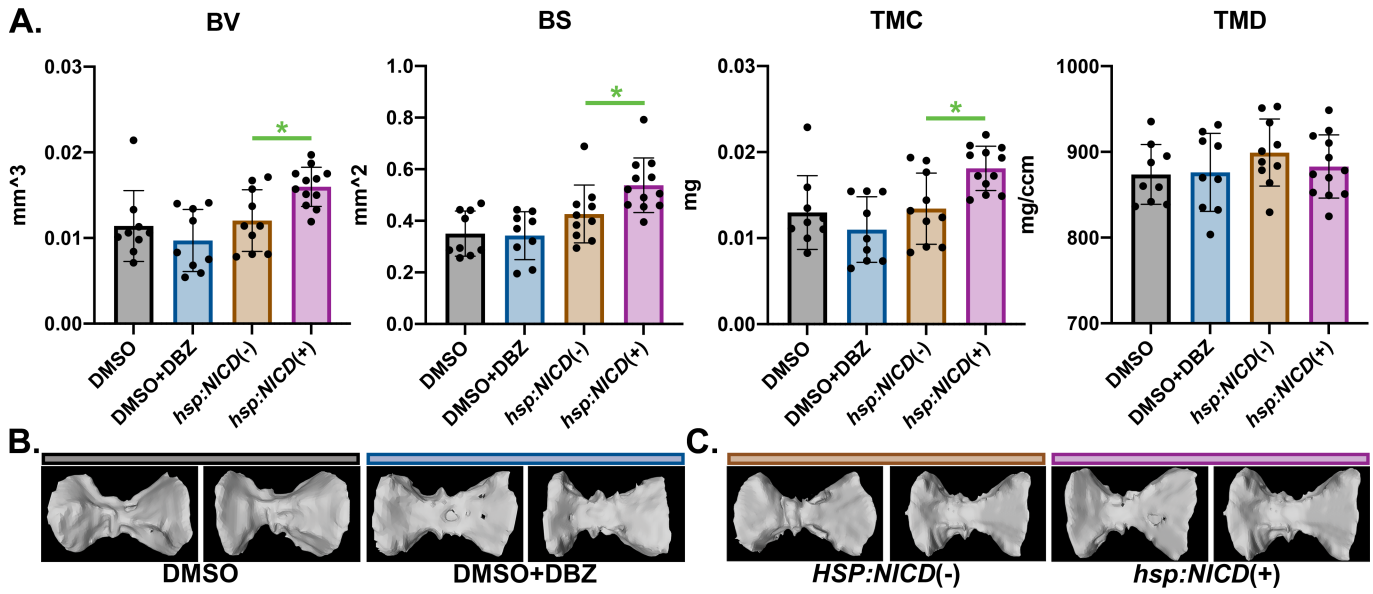


Fig. S2. Notch overactivation promotes vertebral bone accrual. μ CT of the first precaudal/thoracic (T1) vertebral body reveals off-target bone accrual following heat shock treatments in *hsp:NICD+* animals relative to other groups. (A) As in the mandible, *hsp:NICD+* animals acquire increased bone quantity but not density. BV was increased $32.8 \pm 19.0\%$ ($p=0.009$), BS was increased $26.1 \pm 24.8\%$ ($p=0.028$), and TMC was increased $34.9 \pm 19.2\%$ ($p=0.007$) in the *hsp:NICD+* group relative to the *hsp:NICD(-)* group. There was no vertebral phenotype in the DBZ group relative to the DMSO group. The 4 groups represent 9, 9, 10, and 12 animals, in order. (B-C) Two representative μ CT surface renderings are shown for each group. Each graphed datapoint represents an individual fish, with bars depicting means and standard deviations. Green lines/asterisks represent statistical significance ($p < 0.05$) using two-tailed t-tests with Welch's correction.

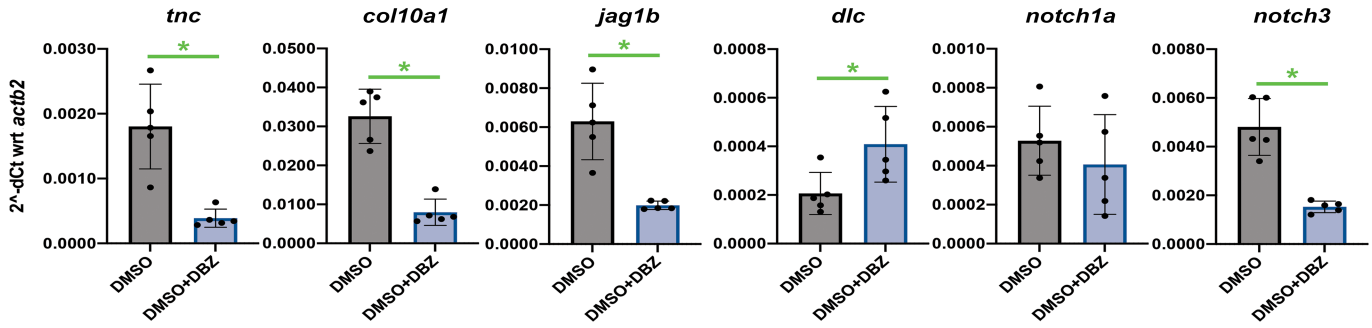


Fig. S3. Callus gene expression changes with DBZ treatment. (A) Whole-callus qPCR at 10 dpr in DMSO versus DMSO+DBZ treatment groups, continued from **Fig. 3D**. Each point represents a different pool of least 11 animals (n=5 pools in each group), with bars depicting means and standard deviations. Green lines/asterisks represent statistical significance (p<0.05) using two-tailed t-tests with Welch's correction.

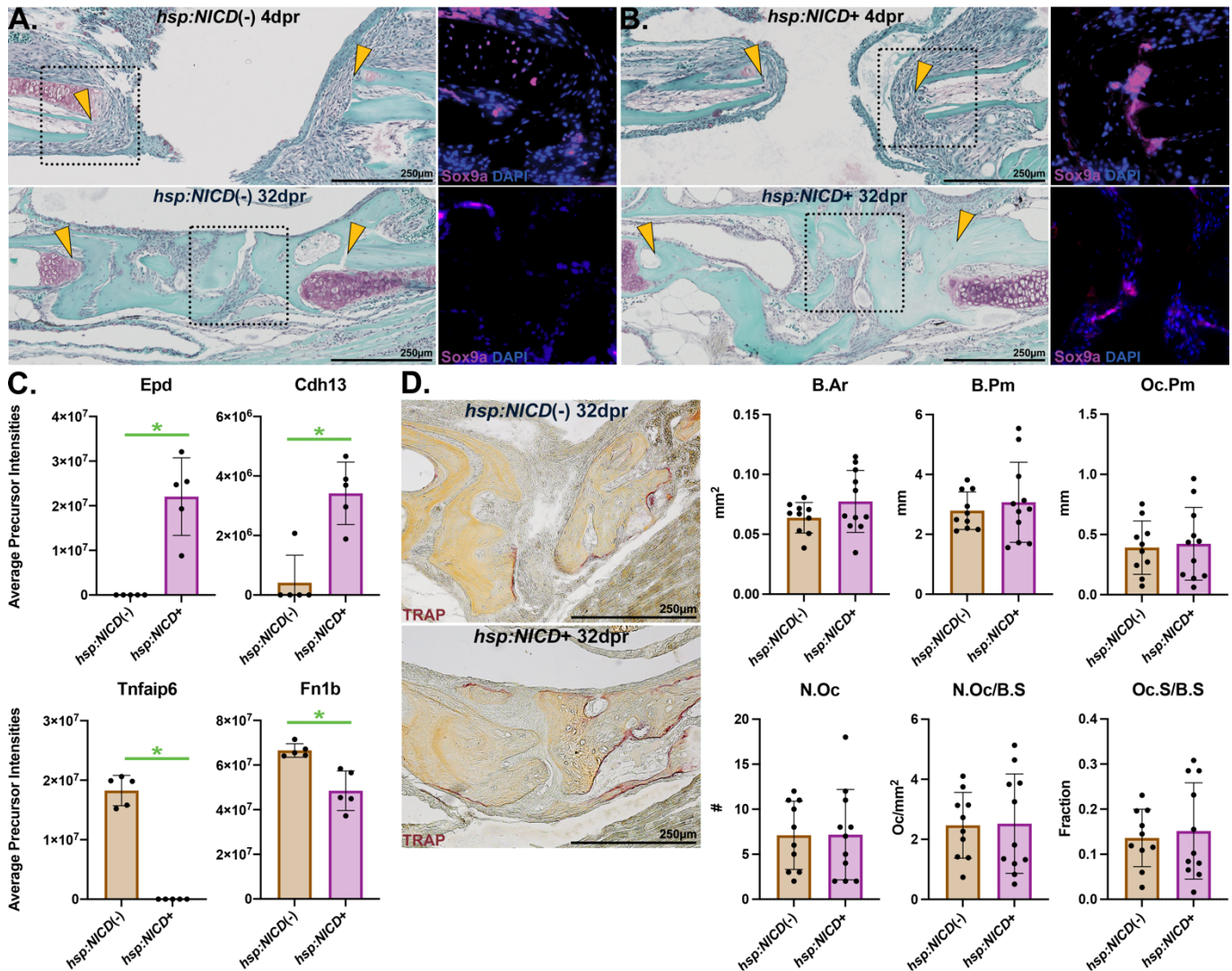


Fig. S4. Changes in mandible callus physiology by Notch overactivation. (A-B) Safranin O histology from *hsp:NICD* \pm animals show an absence of cartilage in both groups at 32 dpr, and more bone present in the *hsp:NICD* $^{+}$ group (quantified by μ CT in **Fig. 2**). The initial cellular response is positive for Sox9a. (C) Changes in the NICD $^{+}$ callus proteome (continued from **Fig. 4**) include factors and extracellular matrix components associated with osteogenesis. Top hits include proteins with known functions in bone, such as the extracellular glycoprotein, ependymin (*Epd*; present only in all 5 *hsp:NICD* $^{+}$ samples, $p < 0.001$) (Pippin et al., 2021; Wagley et al., 2020), and the cell adhesion molecule, cadherin 13 (*Cdh13*; increased 8.3-fold, $p = 0.001$) (Cheng et al., 1998; Yang et al., 2020). Tumor necrosis factor, alpha-

induced protein 6 (Tnfaip6; present only in all 5 *hsp:NICD(-)* samples, $p < 0.001$), also known as Tsg6, an inflammation-induced secreted protein that sequesters BMP2 to inhibit osteoblast and odontoblast differentiation (Mahoney et al., 2008; Wang et al., 2020), was dramatically downregulated in the *hsp:NICD+* calluses. Fibronectin (Fn1b; $p = 0.003$) and numerous collagens were downregulated in the *hsp:NICD+* group. (D) TRAP⁺ osteoclasts are present at 32 dpr in both groups, but histomorphometry was unremarkable for changes caused by NICD. Each graphed datapoint represents an individual fish, with bars depicting means and standard deviations ($n = 5$ per group for proteomics, $n = 10$ and 11 per group for TRAP). Green lines/asterisks represent statistical significance ($p < 0.05$) using two-tailed t-tests with Welch's correction.

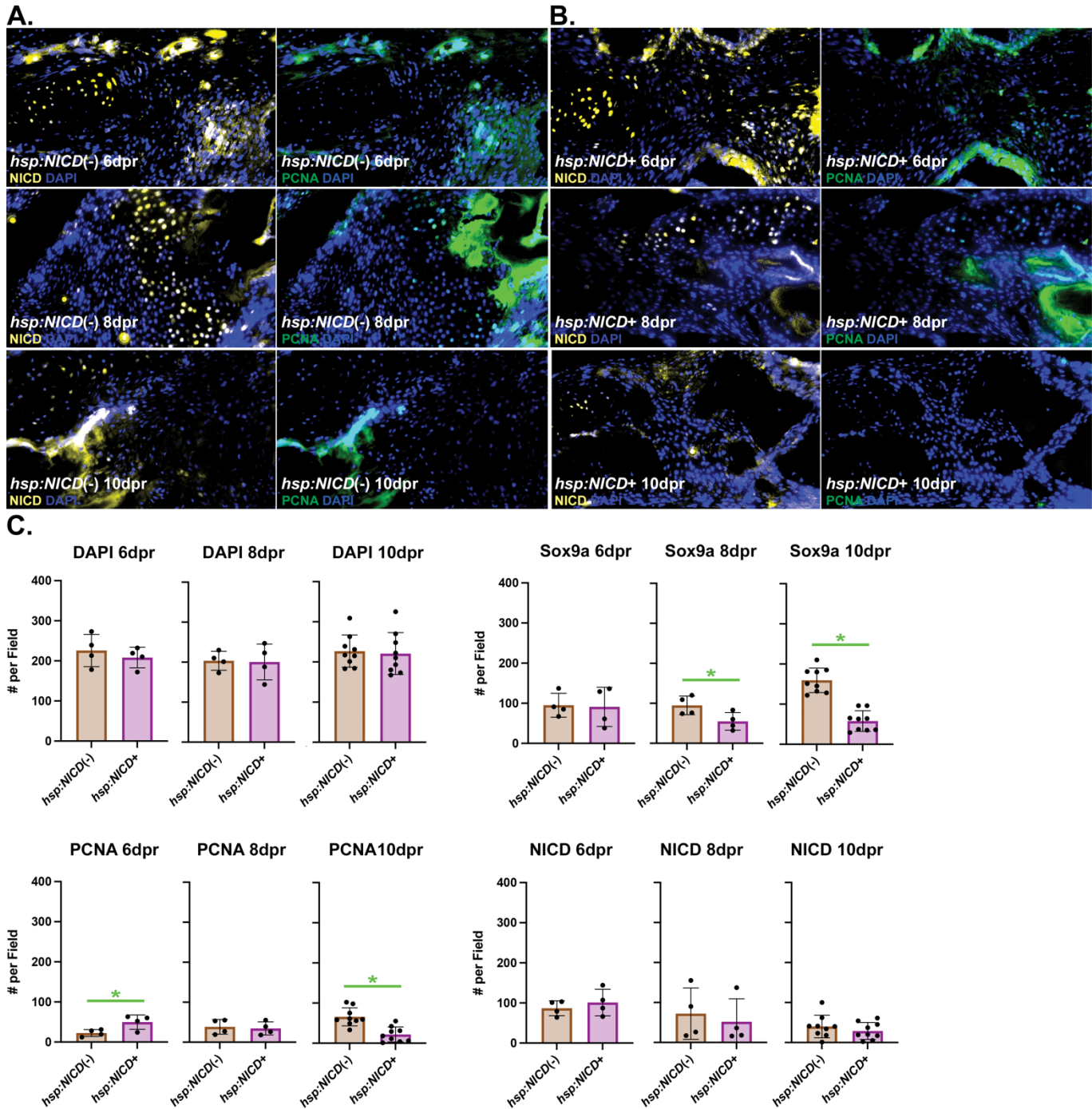


Fig. S5. A subpopulation of Sox9a+/NICD+ cells are proliferative. (A-B) α-NICD IHC (left column) and α-PCNA IHC (right column) from *hsp:NICD±* animals from the same sections and at the same magnification as α-Sox9a IHC in **Fig. 4**. All PCNA+ cells co-stain for NICD, but not all NICD+ cells co-stain for PCNA. (C) Quantitation of IHC shows decreased Sox9a positivity and altered PCNA

kinetics in the NICD⁺ group. The short half-life of NICD (Ilagan et al., 2011) resulted in a lack of detection of the ubiquitous transgene. Each graphed datapoint represents an individual fish, with bars depicting means and standard deviations (n=4 per group at 6 and 8 dpr, n=9 per group at 10 dpr). Green lines/asterisks represent statistical significance ($p < 0.05$) using two-tailed t-tests with Welch's correction.

Table S1. qPCR primers. Forward and reverse primers for use with SYBR Green chemistry. The following abbreviations are used: *actb2* is β -actin 2, *bglap* is osteocalcin, *coll10a1a* is collagen type X α 1a, *colla2* is collagen type II α 2, *dla* is delta-like A, *dlb* is delta-like B, *dlc* is delta-like C, *dld* is delta-like D, *dll4* is delta-like 4, *her6* is hairy-related 6, *jag1a* is Jagged-1a, *jag1b* is Jagged-1b, *jag2a* is Jagged-2a, *jag2b* is Jagged-2b, *notch1a* is Notch receptor 1a, *notch1b* is Notch receptor 1b, *notch2* is Notch receptor 2, *notch3* is Notch receptor 3, *pcna* is proliferating cell nuclear antigen, *sox9a* is SRY-box transcription factor 9a, *sp7* is osterix, *spp1* is osteopontin, and *tnc* is tenascin C.

Gene	NCBI Accession	Forward Primer	Reverse Primer
<i>actb2</i>	NM_181601.5	GCAGAAGGAGATCACATCCCTGGC	CATTGCCGTCACTTCACCGTTC
<i>bglap</i>	NM_001083857.3	TGAGTGCTGCAGAATCTCCTAA	GTCAGGTCTCCAGGTGCAGT
<i>coll10a1a</i>	NM_001083827.1	CCTGTCTGGCTCATACCACA	AAGGCCACCAGGAGAAGAAG
<i>colla2</i>	NM_182968.2	CTGGCATGAAGGGACACAG	GGGGTTCCATTTGATCCAG
<i>dla</i>	NM_130954.2	CTGTGAGAAACCTGGCGAGT	TCCATGTCAGTGCAGCTTCC
<i>dlb</i>	NM_130958.1	CTGTTGCAGTTGGTGGCTTC	CCAGACGACACTTGCCTCT
<i>dlc</i>	NM_130944.1	CATATTACCTGAGCCGCCGT	TCAAAGAGACGATTCCCGGC
<i>dld</i>	NM_130955.2	ACCCTTGCTCGAATGATGCT	CGCCGATCAGCACTAAAAGC
<i>dll4</i>			CTAAGCCAACGGCCAGAGAA
<i>her6</i>	NM_131079.2	GCTTGGGTCAGCTGAAAACG	GTGTTTAGGGCAGCGGTCAT
<i>jag1a</i>	NM_131861.1	GATGCGGGTATGTGAGGCTT	AGTGTGCCACAGGTGTTCAA
<i>jag1b</i>	NM_131863.2	AGAAAGCGTACCACTCTGGC	CCTTGTCTGCAGATCGCTGT
<i>jag2a</i>	XM_689725.8	GGCGGGACCGAACTGTAATA	GTTTCATGGCTGTGTTGCAGG
<i>jag2b</i>	NM_131862.1	TCCCCTTGCCTAAAGACAT	TTTACGCAAGGCTTCCCAT
<i>notch1a</i>	NM_131441.1	GCCCGGATGGTCAGGTAATA	CTCATTAAATGCAGGTGCCGC
<i>notch1b</i>	NM_131302.2	ACACAAGGCCTGGAGTGTTTC	CACAAATTCCTGCCGACCTG
<i>notch2</i>	NM_001115094.2	TCTAGACCAGGTCAGCCGAT	TTGAAACCTGCAAACCCAGG
<i>notch3</i>	NM_131549.2	CCACGTTGCCAGTATCCAGT	TTTGCAGTAGTGCGTGTTC
<i>sox9a</i>	NM_131643.1	GGAGCTCAGCAAACTCTGG	AGTCGGGGTGATCTTTCTTG
<i>sp7</i>	NM_212863.2	GCGGCATCTATATTGGAGGA	AATCTCGGACTGGACTGGTG
<i>spp1</i>	NM_001002308.1	TGAAACAGATGAGAAGGAAGAGG	GGGTAGCCCAAACCTGTCTCC
<i>tnc</i>	NM_130907.2	TTGGAGAAGGCCGGTTGCTAAAT	CAGGGTTCAGGCCAGTCAGGATG

Table S2. Antibodies. Lot numbers for antibodies used, listed in order of first appearance in Histology Methods. All primaries used at 1:250 dilution, all secondaries used at 1:500 dilution.

Antibody	Lot
Novus NBP2-25158	7670-3
Abcam AB175477	GR3261221-8
GeneTex GTX48504	822101530
Sigma-Aldrich MoBU-1	3501021
BD Biosciences 559565	0349390
GeneTex GTX128370	41339
Invitrogen 13-3900	VS292226
Abcam A32849	WA307590
Abcam A11011	2277758
Abcam A11001	2284614
Abcam A11008	2284595
Abcam A32787TR	WI337286

Supplementary Methods

Proteomics

A 200 μg aliquot was removed from each total protein isolation and prepared for proteomics analysis via ultra-high performance liquid chromatography coupled to tandem mass spectrometry (UPLC-MS/MS) using a slightly modified Filter-Aided Sample Preparation protocol (Mara et al., 2020; Wisniewski et al., 2009). Briefly, proteins were diluted with UA buffer (8 M urea in 0.1 M Tris HCl, pH 8.5) and reduced with 25 mM dithiothreitol for 1.5 hr. The reduced protein aliquots were loaded onto Microcon YM-10 10 kD molecular weight cut-off filters pre-conditioned with bovine serum albumin (Sigma-Aldrich) and washed extensively. The filters were spun at 14,000 g for 40 min, the proteins were washed with a 200 μL aliquot of UA buffer, and then subject to another identical round of centrifugation. Proteins were then alkylated with 50 mM iodoacetamide in UA buffer for 15 min in the dark and centrifuged at 14,000 x g for 30 min. Proteins were equilibrated in UB buffer (8 M urea in 0.1 M Tris HCl, pH 8.0) via two consecutive wash and centrifugation steps at 14,000 x g for 30 min. Proteins were then resuspended in 40 μL UB buffer and placed into a new 1.5 mL Eppendorf Safe-Lock tube. The filters were washed twice with 40 μL aliquots of 0.1 M ammonium bicarbonate in water (Fisher Scientific) and washes were combined with the previously removed aliquot. All proteins were digested with endoproteinase LysC (Pierce) at a 1:50 (w/w) enzyme:protein ratio

for 16 hr at 37°C. Samples were then diluted to yield urea concentrations <1 M using 0.1 M ammonium bicarbonate in water and further digested with trypsin (1:50 enzyme:protein, w/w) for 6 hr at 37°C. Fully digested peptides were acidified using formic acid (Fisher Scientific) and subjected to desalting using Pierce C18 Peptide Desalting Spin Columns according to manufacturer's instructions. Dried peptides were resuspended in 0.1% formic acid in water and quantified using a NanoDrop One Spectrophotometer (Thermo Scientific, A280 reading, 1 Abs = 1.0 mg/mL).

Peptide samples were analyzed via UPLC-MS/MS using an UltiMate 3000 RSLCnano UPLC system coupled to a Q Exactive HF mass spectrometer (Thermo Scientific). A 180 min, 300 nL/min, linear reversed phase binary gradient (Solvent A: 0.1% formic acid in water, Solvent B: 0.1% formic acid in acetonitrile) was used to elute peptides directly into the Q Exactive HF instrument via positive mode electrospray ionization with +1.5 kV capillary voltage. The mass spectrometer was operated using the following parameters for precursor MS spectra: mass range 300 to 1800 m/z, 60,000 resolution, AGC target of 1e6, maximum ion time for 60 ms. A Top15 data-dependent mode for MS/MS acquisition used the following parameters: 15,000 resolution, AGC target of 1e5, isolation window of 2.0 m/z, normalized collision energy of 27, charge exclusion for unassigned, +1 and >+8 charge states, and a 30 s dynamic exclusion window.

All raw data were searched against the *Danio rerio* Uniprot reference proteome (UP000000437, accessed 05/17/2021, updated 01/29/2021) using MaxQuant (v1.6.10.43)(Cox and Mann, 2008). MaxQuant parameters included the following: trypsin enzyme specificity, minimum peptide length of 5 amino acids, maximum missed cleavage value of 2, PSM and Protein False Discovery Rate filters of 1%, variable modifications: oxidation of Met, acetylation of protein N-terminus, deamidation of Gln and Asn, and peptide N-terminal Gln to pyroGlu, plus a fixed modification of carbamidomethylation of Cys. All other parameters were left at default values. Label-free quantitation was achieved using the MaxLFQ algorithm. Maxquant output files were uploaded into Scaffold Q+S (v 5.0.0., Proteome Software Inc.) for visualization and further analysis.

In GOrilla, 69.7% of all input targets had a recognized GO term in the March 6, 2021 database. Enrichment score is equal to $(b/n)/(B/N)$, where N is the total number of proteins, B is the total number of proteins associated with a specific GO term, n is the number of significantly dysregulated proteins, and b is the number of dysregulated proteins within a specific GO term.

Supplementary References

- Cheng, S. L., Lecanda, F., Davidson, M. K., Warlow, P. M., Zhang, S. F., Zhang, L., Suzuki, S., St. John, T. and Civitelli, R. (1998). Human Osteoblasts Express a Repertoire of Cadherins, Which Are Critical for BMP - 2-Induced Osteogenic Differentiation. *J Bone Miner Res* 13, 633-644.
- Cox, J. and Mann, M. (2008). MaxQuant enables high peptide identification rates, individualized ppb-range mass accuracies and proteome-wide protein quantification. *Nat Biotechnol.* 26, 1367-1372. doi:10.1038/nbt.151
- Ilgan, M. X., Lim, S., Fulbright, M., Piwnica-Worms, D. and Kopan, R. (2011). Real-time imaging of notch activation with a luciferase complementation-based reporter. *Sci Signal* 4, rs7.
- Mahoney, D. J., Mikecz, K., Ali, T., Mabileau, G., Benayahu, D., Plaas, A., Milner, C. M., Day, A. J. and Sabokbar, A. (2008). TSG-6 regulates bone remodeling through inhibition of osteoblastogenesis and osteoclast activation. *J Biol Chem* 283, 25952-25962.
- Mara, A. B., Gavitt, T. D., Tulman, E. R., Geary, S. J. and Szczepanek, S. M. (2020). Lipid moieties of *Mycoplasma pneumoniae* lipoproteins are the causative factor of vaccine-enhanced disease. *NPJ Vaccines* 5, 1-5.
- Pippin, J A., Chesi, A., Wagley, Y., Su, C., Pahl, M. C., Hodge, K. M., Johnson, M. E., Wells, A. D., Hankenson, K. D. and Grant, S. F. (2021) CRISPR-Cas9-mediated genome editing confirms EPDR1 as an effector gene at the BMD GWAS-implicated 'STARD3NL' locus. *JBMR Plus* 5:9.
- Wagley, Y., Chesi, A., Acevedo, P. K., Lu, S., Wells, A. D., Johnson, M. E., Grant, S. F. and Hankenson, K. D. (2020). Canonical Notch signaling is required for bone morphogenetic protein-mediated human osteoblast differentiation. *Stem Cells* 38, 1332-1347.

- Wang, Y., Yuan, S., Sun, J., Gong, Y., Liu, S., Guo, R., He, W., Kang, P. and Li, R. (2020). Inhibitory effect of the TSG-6 on the BMP-4/Smad signaling pathway and odonto/osteogenic differentiation of dental pulp stem cells. *Biomed Pharmacother* 128, 110266.
- Wisniewski, J. R., Zougman, A., Nagaraj, N. and Mann, M. (2009). Universal sample preparation method
- Yang, Y. R., Kabir, M. H., Park, J. H., Park, J.-I., Kang, J. S., Ju, S., Shin, Y. J., Lee, S. M., Lee, J. and Kim, S. (2020). Plasma proteomic profiling of young and old mice reveals cadherin-13 prevents age-related bone loss. *Aging* 12, 8652.